Adaptive backstepping with magnitude, rate, and bandwidth constraints: Aircraft longitude control

Jay Farrell[†], Marios Polycarpou[‡], and Manu Sharma[§]

[†] Department of Electrical Engineering, University of California, Riverside, CA 92521 USA

[‡] Dept. of Elect. and Comp. Engineering and Computer Science, Univ. of Cincinnati, Cincinnati, OH 45221, USA

[§] Barron Associates, Inc., 1160 Pepsi Place, Suite 300, Charlottesville, Virginia 22901

Abstract

This article presents an adaptive backstepping approach to the longitudinal (γ, α, Q) control of an aircraft that directly accommodates magnitude, rate, and bandwidth constraints on the aircraft states and the actuator signals. The article includes design of the control law, Lyapunov analysis of the stability properties of the closed loop system, and simulation based analysis of the performance.

1 Introduction

The introduction of uninhabited combat air vehicles (UCAV's) has generated interest in adaptive control for aircraft that are capable of maintaining trajectory following control even subsequent to faults or battle damage. In addition, physical limitations impose magnitude, rate, and bandwidth constraints on the control surface deflections and the aircraft states. In this article, we present analysis and simulation results for an adaptive backstepping approach that is designed to accommodate magnitude, rate, and bandwidth constraints on the actuator signals as well as the intermediate control variables used in the backstepping control approach.

Adaptive control has been applied to aircraft in, for example [2, 3, 4, 14, 15, 18]. Piloted hardware in the loop simulation and flight testing is described in [2, 4, 18]. The approach of [3, 4] used a dynamic inversion based nonlinear controller with a neural network approximating the error in the inversion process. Adaptive backstepping has been applied to aircraft in for example [15]. That article did not consider the effects of saturation on the closed loop performance.

Control signal rate and amplitude constraints in adaptive control are addressed in, for example, [1, 7, 9, 10, 17]. The first type of method is to completely stop adaptation under saturation conditions. This ad-hoc method does prevent the tracking errors induced by actuator constraints from corrupting the parameter adaptation, but is undesirable as it does not allow any theoretical stability guarantees. The second set of approaches (training signal hedging (TSH)), see e.g. [1, 9], corrects the tracking error only where it is used in the parameter adaptation laws. It does not directly change the reference input to the control loop. The third set of of techniques, referred to as pseudo-control hedging (PCH) [7, 10], only alters the commanded input to the loop. The goal in PCH is to decrease the command to the loop to a point where it is implementable without saturation. PCH does not directly change the signal used in the parameter adaptation laws. The work in [7] develops and analyzes the PCH method to extend the control approach of [3, 14] to accommodate magnitude and rate limits on the commanded surface deflections. Although the second and third approaches start with radically different philosophies, for first order systems, it can be shown that these two approaches are identical. For higher order or nonlinear systems, the comparison is not as straightforward.

This article presents an adaptive backstepping approach for longitudinal control of an aircraft that has state and actuator constraints. Both theoretical and simulation analyses are included. A novel aspect of this approach is the ability to accommodate magnitude, rate, and bandwidth constraints on the actuator signals and each of the intermediate control variables (i.e., aircraft state variables) used in the backstepping design. This result is of interest in its own right. This approach has similarities with both the TSH and PCH methods, since it corrects both the training signal and the reference input at each step of the backstepping procedure. Our ultimate goal is to extend this approach to a full vehicle controller using on-line function approximation [5, 11, 12] to accommodate battle damage types of events.

2 Problem Formulation

Due to space limitations, the discussion of this article will focus on a simplified aircraft model with the same structure as the linearized, rigid body, aircraft longitudinal dynamics [16]. The model is just complex enough to allow a presentation and analysis of the control design approach. Since the model has the same structure as aircraft longitudinal dynamics, the approach can be extended to a realistic nonlinear aircraft model. This extension is discussed further in the conclusions section.

Report Documentation Page

Form Approved
OMB No. 0704-0188

Public reporting burden for the collection of information is estimated to average 1 hour per response, including the time for reviewing instructions, searching existing data sources, gathering and maintaining the data needed, and completing and reviewing the collection of information. Send comments regarding this burden estimate or any other aspect of this collection of information, including suggestions for reducing this burden, to Washington Headquarters Services, Directorate for Information Operations and Reports, 1215 Jefferson Davis Highway, Suite 1204, Arlington VA 22202-4302. Respondents should be aware that notwithstanding any other provision of law, no person shall be subject to a penalty for failing to comply with a collection of information if it does not display a currently valid OMB control number.

1. REPORT DATE **2006**	2. REPORT TYPE	3. DATES COVERED **00-00-2006 to 00-00-2006**
4. TITLE AND SUBTITLE **Adaptive backstepping with magnitude, rate, and bandwidth constraints: Aircraft longitude control**		5a. CONTRACT NUMBER
		5b. GRANT NUMBER
		5c. PROGRAM ELEMENT NUMBER
6. AUTHOR(S)		5d. PROJECT NUMBER
		5e. TASK NUMBER
		5f. WORK UNIT NUMBER
7. PERFORMING ORGANIZATION NAME(S) AND ADDRESS(ES) **Air Force Research Laboratory,Wright Patterson AFB,OH,45433**		8. PERFORMING ORGANIZATION REPORT NUMBER
9. SPONSORING/MONITORING AGENCY NAME(S) AND ADDRESS(ES)		10. SPONSOR/MONITOR'S ACRONYM(S)
		11. SPONSOR/MONITOR'S REPORT NUMBER(S)
12. DISTRIBUTION/AVAILABILITY STATEMENT **Approved for public release; distribution unlimited**		
13. SUPPLEMENTARY NOTES		
14. ABSTRACT **see report**		
15. SUBJECT TERMS		

16. SECURITY CLASSIFICATION OF:			17. LIMITATION OF ABSTRACT	18. NUMBER OF PAGES	19a. NAME OF RESPONSIBLE PERSON
a. REPORT **unclassified**	b. ABSTRACT **unclassified**	c. THIS PAGE **unclassified**		**7**	

Standard Form 298 (Rev. 8-98)
Prescribed by ANSI Std Z39-18

The model that we will consider has the form

$$\begin{aligned}\dot{\gamma} &= L_o + L_\alpha \alpha \\ \dot{\alpha} &= Q - (L_o + L_\alpha \alpha) \\ \dot{Q} &= M_o + M_Q Q + M_\delta \delta,\end{aligned}$$

where the (normalized[1]) lift force is modeled as $L_o + L_\alpha \alpha$ and the (normalized[2]) pitch moment is modeled as $M_o + M_Q Q + M_\delta \delta$. In this expression, γ is the flight path angle, α is the angle of attack, Q is the pitch rate, and δ is the control surface deflection. At an operating point, L_o, L_α, M_o, M_Q and M_δ are unknown, constant, scalar parameters. Additional terms can be added to the lift or moment models without changing the theoretical approach. Most importantly, the approach directly extends to the case where multiple independent surfaces are available. These generalizations are not included here due to space limitations.

The corresponding tracking error dynamic equations are

$$\begin{aligned}\dot{\tilde{\gamma}} &= L_o + L_\alpha (\alpha_c + \tilde{\alpha}) - \dot{\gamma}_c \\ \dot{\tilde{\alpha}} &= -(L_o + L_\alpha \alpha) + Q_c + \tilde{Q} - \dot{\alpha}_c \\ \dot{\tilde{Q}} &= M_o + M_Q Q + M_\delta \delta - \dot{Q}_c\end{aligned}$$

where the tracking errors are defined as $\tilde{\gamma} = \gamma - \gamma_c$, $\tilde{\alpha} = \alpha - \alpha_c$, $\tilde{Q} = Q - Q_c$.

Our goal is to generate a backstepping controller that will cause γ to track an input signal γ_c. We assume that γ_c is smooth and that $\dot{\gamma}_c$ is known. In the backstepping approach, the γ controller will generate a commanded value α_c^0 for α. An α controller will generate a Q_c^0 command for Q. The Q controller will generate the control surface command δ_c^0 to achieve the Q command.

Since an aircraft operating envelope includes constraints on both actuators and states, the controller must work in the presence of magnitude, rate, and bandwidth limits on δ as well as operating envelope constraints on Q and α. In the formulation to follow, we will treat $(L_o, L_\alpha, M_o, M_Q, M_\delta)$ as parameters to be identified. Therefore, we are implementing adaptive backstepping with control variable and state constraints. In the actual application, this set of linearization 'parameters' is a function of the operating conditions. Since the operating condition is slowly time varying, the adaptive laws would be required to adapt the parameters to match the local model. In the final full vehicle implementation, these 'linearized parameters' would be approximated as a function of the flight condition.

[1] To simplify the notation, the $\frac{1}{mV}$ factor at the operating point is included in the lift function.

[2] To simplify the notation, the $\frac{1}{I_{yy}}$ factor is included in the moment function.

3 Adaptive Backstepping with Saturation

The backstepping control laws are summarized below. The operating envelope requires α to remain in the interval $[\alpha_c^L, \alpha_c^U]$ and Q to remain in the interval $[Q_c^L, Q_c^U]$. The actuator design requires δ to remain in the interval $[\delta_c^L, \delta_c^U]$. In addition, the actuator design will impose rate and bandwidth limitations on δ, which in turn will result in rate and bandwidth limitations on the intermediate variables Q_c and α_c. The above operating envelope and surface deflection constraints are assumed to be known and fixed.

The nominal backstepping commands are

$$\begin{aligned}\alpha_c^0 &= \frac{1}{\hat{L}_\alpha}\left(-\hat{L}_o + \dot{\gamma}_c - k_\gamma\, \tilde{\gamma} + \eta_\gamma\right) - \chi_\alpha \\ Q_c^0 &= \left(\hat{L}_o + \hat{L}_\alpha \alpha\right) - k_\alpha \tilde{\alpha} + \eta_\alpha + \dot{\alpha}_c - \bar{\gamma}\hat{L}_\alpha - \chi_Q \\ \delta_c^0 &= \frac{1}{\hat{M}_\delta}\left(-\hat{M}_o - \hat{M}_Q Q - k_Q \tilde{Q} + \eta_Q - \bar{\alpha} + \dot{Q}_c\right)\end{aligned}$$

with $k_\gamma, k_\alpha, k_Q > 0$. The robustifying terms $(\eta_\gamma, \eta_\alpha, \eta_Q)$ are motivated in the proof of the theorem to follow. The amplitude, rate, and bandwidth limited control signals can be defined by

$$\begin{aligned}e_\alpha &= \left(sat\left(\alpha_c^0, \alpha_c^L, \alpha_c^U\right) - x_{\alpha_1}\right) \\ \begin{bmatrix} \dot{x}_{\alpha_1} \\ \dot{x}_{\alpha_2} \end{bmatrix} &= \begin{bmatrix} 0 & 1 \\ 0 & -2\zeta_\alpha \omega_{n_\alpha} \end{bmatrix} \begin{bmatrix} x_{\alpha_1} \\ x_{\alpha_2} \end{bmatrix} \\ &\quad + \begin{bmatrix} 0 \\ \omega_{n_\alpha}^2 \end{bmatrix} sat(e_\alpha, -L_\alpha, L_\alpha) \\ \begin{bmatrix} \alpha_c \\ \dot{\alpha}_c \end{bmatrix} &= \begin{bmatrix} 1 & 0 \\ 0 & 1 \end{bmatrix} \begin{bmatrix} x_{\alpha_1} \\ x_{\alpha_2} \end{bmatrix}\end{aligned}$$

where the parameters of this filter are defined below. In this filter, e_α is the error between the first filter state and the magnitude limited filter input. Since the first state of the filter is used in the computation of e_α, the characteristic equation of the filter is $s^2 + 2\zeta_\alpha \omega_{n_\alpha} s + \omega_{n_\alpha}^2 = 0$, in the linear portion of the two *sat* functions. The *sat* function in the second equation enforces the rate limit. At the filter output, α_c is magnitude, rate, and bandwidth limited. The command filters for Q_c and δ_c are defined similarly as

$$\begin{aligned}e_Q &= \left(sat\left(Q_c^0, Q_c^L, Q_c^U\right) - x_{Q_1}\right) \\ \begin{bmatrix} \dot{x}_{Q_1} \\ \dot{x}_{Q_2} \end{bmatrix} &= \begin{bmatrix} 0 & 1 \\ 0 & -2\zeta_Q \omega_{n_Q} \end{bmatrix} \begin{bmatrix} x_{Q_1} \\ x_{Q_2} \end{bmatrix} \\ &\quad + \begin{bmatrix} 0 \\ \omega_{n_Q}^2 \end{bmatrix} sat(e_Q, -L_Q, L_Q) \\ \begin{bmatrix} Q_c \\ \dot{Q}_c \end{bmatrix} &= \begin{bmatrix} 1 & 0 \\ 0 & 1 \end{bmatrix} \begin{bmatrix} x_{Q_1} \\ x_{Q_2} \end{bmatrix}\end{aligned}$$

$$
\begin{aligned}
e_\delta &= \left(sat\left(\delta_c^0, \delta_c^L, \delta_c^U\right) - x_{\delta_1}\right) \\
\begin{bmatrix} \dot{x}_{\delta_1} \\ \dot{x}_{\delta_2} \end{bmatrix} &= \begin{bmatrix} 0 & 1 \\ 0 & -2\zeta_\delta \omega_{n_\delta} \end{bmatrix} \begin{bmatrix} x_{\delta_1} \\ x_{\delta_2} \end{bmatrix} \\
&\quad + \begin{bmatrix} 0 \\ \omega_{n_\delta}^2 \end{bmatrix} sat(e_\delta, -L_\delta, L_\delta) \\
\begin{bmatrix} \delta_c \end{bmatrix} &= \begin{bmatrix} 1 & 0 \end{bmatrix} \begin{bmatrix} x_{\delta_1} \\ x_{\delta_2} \end{bmatrix}.
\end{aligned}
$$

In these expressions, $L_\alpha = \frac{2\zeta_\alpha R_\alpha}{\omega_{n_\alpha}^2}$, $L_Q = \frac{2\zeta_Q R_Q}{\omega_{n_Q}^2}$, $L_\delta = \frac{2\zeta_\delta R_\delta}{\omega_{n_\delta}^2}$ and $(R_\alpha, R_Q, R_\delta)$ are rate limits on (α, Q, δ), respectively; $(\omega_{n_\alpha}, \omega_{n_Q}, \omega_{n_\delta})$ are bandwidth limits on (α, Q, δ); $(\alpha_c^U, Q_c^U, \delta_c^U)$ are upper limits on (α, Q, δ); $(\alpha_c^L, Q_c^L, \delta_c^L)$ are lower limits on (α, Q, δ), and *sat* denotes the saturation function that is linear with unity slope between its lower and upper limits. This paragraph has presented one command filter approach, many other filters are possible without affecting the validity of the stability proofs. If the surface position can be measured, then the last filter is not required. Also the parameters of the above filters are not completely independent. For example, since the derivative of α is closely related to Q, the rate limit R_α should be less than or equal to the magnitude limit Q_c^U.

The vector $\chi = [\chi_\gamma(t), \chi_\alpha(t), \chi_Q(t)]$ is generated by

$$
\begin{aligned}
\dot{\chi}_\gamma &= -k_\gamma \chi_\gamma + \hat{L}_\alpha \left(\alpha_c - \alpha_c^0\right) \\
\dot{\chi}_\alpha &= -k_\alpha \chi_\alpha + \left(Q_c - Q_c^0\right) \\
\dot{\chi}_Q &= -k_Q \chi_Q + \hat{M}_\delta \left(\delta_c - \delta_c^0\right).
\end{aligned}
$$

These signals are filtered versions of the effect of state and control rate, bandwidth, and magnitude constraints on the variable that is being controlled. Finally, we define the vector of modified tracking errors $\bar{x} = [\bar{\gamma}, \bar{\alpha}, \bar{Q}]$ as

$$
\begin{aligned}
\bar{\gamma} &= \tilde{\gamma} - \chi_\gamma \\
\bar{\alpha} &= \tilde{\alpha} - \chi_\alpha \\
\bar{Q} &= \tilde{Q} - \chi_Q.
\end{aligned}
$$

When there is no control variable saturation, $\bar{x}$ converges to $\tilde{x}$. In the presence of state and control variable constraints, the signal χ is designed to remove the effects of the saturation from $\tilde{x}$ to generated $\bar{x}$, which will be used in the parameter adaptation laws. The parameter adaptation laws are:

$$
\dot{\hat{M}}_o = \Gamma_3 \bar{Q} \qquad \dot{\hat{L}}_o = \Gamma_1 \left(\bar{\gamma} - \bar{\alpha}\right) \tag{1}
$$

$$
\dot{\hat{M}}_Q = \Gamma_4 \bar{Q} Q \qquad \dot{\hat{L}}_\alpha = \Gamma_2 \left(\bar{\gamma} - \bar{\alpha}\right) \alpha \tag{2}
$$

$$
\dot{\hat{M}}_\delta = \Gamma_5 \bar{Q} \delta, \tag{3}
$$

where Γ_i for $i = 1, \ldots, 5$ are positive adaptation gains. The subsequent sections will show that the above control laws are stable even in the presence of state and control rate, bandwidth, and magnitude constraints. In an implementation, deadzones should be used to avoid parameter drift due to noise; and, projection methods must be used to ensure that the estimation transient does not cause $\hat{L}_\alpha$ or $\hat{M}_\delta$ to change sign.

4 Tracking Error Dynamics

Representing the actual parameters as the estimated parameter minus parameter estimation error: $L_o = \hat{L}_o - \tilde{L}_o$, $L_\alpha = \hat{L}_\alpha - \tilde{L}_\alpha$, $M_o = \hat{M}_o - \tilde{M}_o$, $M_Q = \hat{M}_Q - \tilde{M}_Q$, $M_\delta = \hat{M}_\delta - \tilde{M}_\delta$; the dynamics of the modified tracking errors are

$$
\begin{aligned}
\dot{\bar{\gamma}} &= \dot{\tilde{\gamma}} - \dot{\chi}_\gamma \\
&= \left(L_o + L_\alpha \alpha - \dot{\gamma}_c\right) - \left(-k_\gamma \chi_\gamma + \hat{L}_\alpha \left(\alpha_c - \alpha_c^0\right)\right) \\
&= \hat{L}_o + \hat{L}_\alpha \left(\alpha_c^0 + \tilde{\alpha}\right) - \dot{\gamma}_c - \tilde{L}_o - \tilde{L}_\alpha \alpha + k_\gamma \chi_\gamma \\
&= -k_\gamma \bar{\gamma} + \hat{L}_\alpha \bar{\alpha} - \tilde{L}_o - \tilde{L}_\alpha \alpha + \eta_\gamma \qquad (4) \\
\dot{\bar{\alpha}} &= \dot{\tilde{\alpha}} - \dot{\chi}_\alpha \\
&= -k_\alpha \bar{\alpha} + \tilde{L}_o + \tilde{L}_\alpha \alpha - \bar{\gamma} \hat{L}_\alpha + \bar{Q} + \eta_\alpha \qquad (5) \\
\dot{\bar{Q}} &= \dot{\tilde{Q}} - \dot{\chi}_Q \\
&= -k_Q \bar{Q} - \bar{\alpha} - \tilde{M}_o - \tilde{M}_Q Q - \tilde{M}_\delta \delta + \eta_Q. \qquad (6)
\end{aligned}
$$

The final numbered equations will be used in the subsequent stability analysis.

5 Lyapunov Analysis

The objective of this section is to prove the stability of the closed loop system using Lyapunov-like methods. The results are summarized in the following theorem.

Theorem 5.1 *The closed loop system with dynamics described in Section 2 and controller described in Section 3 has the following properties:*

1. $\tilde{L}_o, \tilde{L}_\alpha, \tilde{M}_o, \tilde{M}_Q, \tilde{M}_\delta \in \mathcal{L}_\infty$
2. $\bar{\gamma}$, $\bar{\alpha}$, *and* $\bar{Q} \in \mathcal{L}_\infty$
3. $\bar{\gamma}$, $\bar{\alpha}$, *and* $\bar{Q}$ *converge to zero with* $\bar{\gamma}$, $\bar{\alpha}$, *and* $\bar{Q} \in \mathcal{L}_2$.

In addition, although we do not show it here, it is possible to show that given certain persistence of excitation conditions, the parameter errors converge exponentially to zero.

Proof: Define the γ-Lyapunov function as

$$
\mathcal{V} = \frac{1}{2}\left(\bar{\gamma}^2 + \bar{\alpha}^2 + \bar{Q}^2\right) + \frac{1}{2}\tilde{\Theta}^T \Gamma^{-1} \tilde{\Theta}
$$

where $\Theta^T = [L_o, L_\alpha, M_o, M_Q, M_\delta]$, $\hat{\Theta}$ is the estimate of Θ, and $\tilde{\Theta} = \hat{\Theta} - \Theta$. Taking the time derivative of $\mathcal{V}$, using eqns. (4-6) to eliminate $(\dot{\bar{\gamma}}, \dot{\bar{\alpha}}, \dot{\bar{Q}})$, and using eqns.

(1-3) to eliminate $\dot{\tilde{\Theta}}$, after some algebraic manipulations yields

$$\begin{aligned}\dot{\mathcal{V}} &= -k_Q\bar{Q}^2 - k_\alpha\bar{\alpha}^2 - k_\gamma\bar{\gamma}^2 \\ &\quad +\bar{\gamma}\eta_\gamma + \bar{\alpha}\eta_\alpha + \bar{Q}\eta_Q. \end{aligned} \tag{7}$$

Therefore, the designer selects $(\eta_\gamma, \eta_\alpha, \eta_Q)$ as odd, differentiable functions with sign opposite to $(\bar{\gamma}, \bar{\alpha}, \bar{Q})$, respectively. The magnitude of these robustifying terms would be selected to ensure boundedness of tracking errors in the presence of model error, measurement noise, or disturbances. For the results of Section 6, all three of these terms are set to zero.

Since $\mathcal{V}(t)$ is nonincreasing, we conclude that $(\bar{Q}, \bar{\alpha}, \bar{\gamma}, \tilde{\Theta}^T)$ are each bounded. Barbalat's Lemma implies that the origin of the $(\bar{Q}, \bar{\alpha}, \bar{\gamma})$ variables is asymptotically stable. Finally, because $0 \leq \mathcal{V}(t) \leq \mathcal{V}(0)$, integration of both sides of (7) shows that $(\bar{Q}, \bar{\alpha}, \bar{\gamma}) \in \mathcal{L}_2.\diamondsuit$

This theorem shows that even when the nominal commands $(\alpha_c^0, Q_c^0, \delta^0)$ exceed the state and control limitations, the quantities $\bar{x} = [\bar{\gamma}, \bar{\alpha}, \bar{Q}]^T$ and $\tilde{\Theta}$ do not diverge. In fact, the cumulative norm of these quantities as defined by $\sqrt{\mathcal{V}(t)}$ will never increase. Nothing is proved about the tracking error $\tilde{x}$, which may increase during periods when the state or control limitations are in effect, because the desired control signal is not being implemented (i.e., $u_c \neq u_c^0$). The vector χ is defined to remove from $\tilde{x}$ the portion of the tracking error that is due to violation of the state or control signal limitations. The compensated error $\bar{x}$ is used to adapt the parameters, even during periods in which the state or control signal limitations prevent implementation of the desired control signals. When the state or control signal limitations are not in effect, (i.e., $u_c = u_c^0$), χ approaches zero, and $\tilde{x}$ converges towards $\bar{x}$.

6 Simulation Example

This section analyzes results from a simulation example. The parameters for the simulation were defined in Table 1. The control gains are selected to enforce a time scale separation between the three loops of the backstepping controller. The section contains two sets of results. The first set of results pertain to a situation where saturation does not occur. The second set of results pertain to a situation where significant saturation occurs in all three control loops. The parameters of the command filters defined in Section 3 are $\zeta_\alpha = \zeta_Q = 1$, $\omega_{n_\alpha} = k_\alpha$, and $\omega_{n_Q} = k_Q$.

6.1 Example: No saturation

For this set of simulations, γ_r is a 25s square wave with peak magnitude of ± 5 deg. The commands γ_c and $\dot{\gamma}_c$ are the states of a second order, relative degree two, unity gain prefilter with $\zeta = 1$, and $\omega_n = k_\gamma$.

Figure 1 contains plots of the states and actuator signal for the first and last 25 seconds of a 150 s simulation. Each graph contains three curves. The dotted curve is the command. The solid curve is the magnitude, rate, and bandwidth limited command. The dashed curve is the actual state or actuator variable. Even though the initial parameter error is large, the transient in the control response is reasonable. Figure 2 includes graphs of the three components of $\tilde{x}$ in the left column and the three components of $\bar{x}$ in the right column. Note that as the theory predicted, since there is no saturation, $\tilde{x} \to \bar{x} \to 0$.

The convergence of $\bar{x}$ to zero is not monotonic. However, the Lyapunov function is non-increasing. The left column of Figure 3 plots the norm of the parameter error, the norm of $\bar{x}$, and the norm defined by the square root of the Lyapunov function. Notice that although the norm of $\bar{x}$ is both increasing and decreasing, the Lyapunov function never increases. The right column of Figure 3 plots each component of $\hat{\Theta}$.

6.2 Example: Substantial Saturation

For this set of simulations, γ_r is a 25s square wave with peak magnitude of ± 10 deg. The commands γ_c and $\dot{\gamma}_c$ are the states of a second order, relative degree two, unity gain prefilter with $\zeta = 1$, and $\omega_n = k_\gamma$.

Figure 4 contains plots of the states and actuator signal for the first and last 25 seconds of a 150 s simulation. Even though the initial parameter error is large, the transient in the control response is reasonable. Note that the large γ commands result in rate, magnitude, or bandwidth constraining the α_c, Q_c, and δ_c variables. Figure 5 includes graphs of the three components of $\tilde{x}$ in the left column and the three components of $\bar{x}$ in the right column. Note that as the theory predicted, since there is saturation, $\bar{x} \to 0$, but $\tilde{x}$ does not converge to zero. In spite of this fact, the parameter estimates converge toward the correct values. In fact, as shown in the right column of Figure 6, the parameters converge faster than they did in Figure 3. There is a significantly higher level of excitation in the present example, but the parameter estimates will only converge if the training error is properly compensated to remove the effects of the rate, magnitude, and bandwidth limitations on the control signals. The left column of Figure 6 contains plots of the norm of the parameter error, the norm of $\bar{x}$, and the norm defined by the square root of the Lyapunov function. Note that the Lyapunov function is non-increasing even during the periods of saturation.

7 Conclusions

This article has presented and analyzed an adaptive backstepping approach to the control of longitudinal aircraft dynamics that directly accommodates magnitude, rate, and bandwidth limits on the aircraft states and actuators. For this preliminary analysis, we have only considered a linearized aircraft point design. Due to the positive analysis of the performance, we are cur-

rently extending this research in four directions. First, we are extending the adaptive state and actuator constrained backstepping control approach to include control of lateral-directional dynamics. Second, we are extending the linearized adaptive approach to a nonlinear on-line function approximation based approach [6]. Third, we are extending the theoretical analysis as a general extension of the backstepping approach[13]. Finally, we have extended the results presented herein to the case where the vehicle has multiple, redundant and independent actuators.

8 Acknowledgement

This research supported by University of California–Riverside, and University of Cincinnati, and Barron Associates Inc. through Air Force PRDA 01-03-VAK.

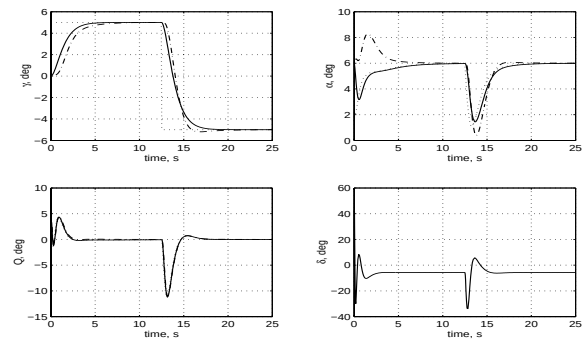

(a) Initial state and control

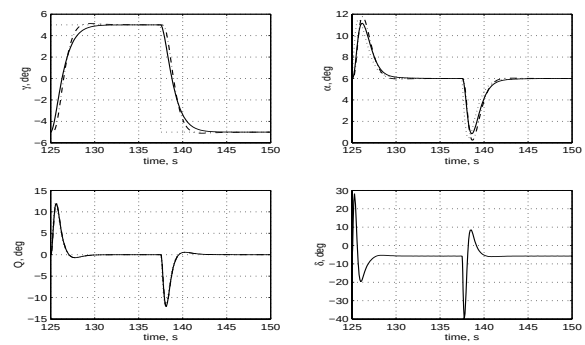

(b) Final state and control

Figure 1: Plots of the aircraft state and control signal at the beginning and end of a 150 s simulation with $\gamma_r \in \pm 5$ deg: command (dotted), filtered command (solid), actual (dashed).

References

[1] A. M. Annaswamy and J. E. Wong. "Adaptive control in the presence of saturation nonlinearity", Int. J. of Adaptive Control and Signal Processing, Vol. 11: 3–19, 1997.

[2] J. Brinker and K. Wise, "Flight testing of a reconfigurable flight control law on the X-36 tailless aircraft," J. of Guidance, Control, and Dynamics, Vol. 24(5): 903–909, 2001.

[3] A. J. Calise, R. T. Rysdyk, "Nonlinear Adaptive Flight Control using Neural Networks," IEEE Control Systems Magazine, pp. 14–25, Dec. 1998.

[4] A. J. Calise, S. Lee, and M. Sharma, "Development of a reconfigurable flight control law for the X-36 tailless aircraft," J. of Guidance, Control, and Dynamics, Vol. 24(5): 896–902, 2001.

[5] J. A. Farrell,"Stability and Approximator Convergence in Nonparametric Nonlinear Adaptive Control," IEEE Trans. on Neural Networks, Vol. 9(5): 1008-1020, 1998.

[6] J. A. Farrell, M. Sharma, and M. Polycarpou, "Longitudinal Flight-path Control using on-line Function Approximation," AIAA J. of Guidance, Control and Dynamics, accepted for publication Jan. 2003.

[7] E. Johnson and A. Calise. "Neural network adaptive control of systems with input saturation," In American Control Conference, June 2001.

[8] M. Krstić, I. Kanellakopoulos, and P. Kokotović, Nonlinear and Adaptive Control Design, New York, John Wiley, 1995.

[9] S. P. Kárason and A. M. Annaswamy. "Adaptive control in the presence of input constraints," IEEE Trans. on Automatic Control, Vol. 39 (11): 2325–2330, 1994.

[10] R. Monopoli. "Adaptive control for systems with hard saturation," In IEEE Conf. on Decision and Control, pp. 841–843, 1975.

[11] M. Polycarpou and P. Ioannou, "A Robust Adaptive Nonlinear Control Design," Automatica, vol. 32(3): 423-427, 1996.

[12] M. Polycarpou and M. Mears, "Stable Adaptive Tracking of Uncertain Systems Using Nonlinearly Parametrized On-Line Approximators," Int. J. of Control, vol. 70(3): 363-384, 1998.

[13] M. Polycarpou, J. A. Farrell, and M. Sharma, "On-Line Approximation Control of Uncertain Nonlinear Systems: Issues with Control Input Saturation" In Proc. of the 2003 American Controls Conference.

[14] R. T. Rysdyk, Adaptive Nonlinear Flight Control, Ph.D. Thesis, Georgia Institute of Technology, School of Aero. Eng., Atlanta, GA, 1998.

[15] S. N. Singh and M. Steinberg, "Adaptive Control of Feedback Linearizable Nonlinear Systems with Application to Flight Control," J. of Guid, Control, and Dynamics, 19(4): 871–877, 1996.

[16] B. L. Stevens and F. L. Lewis, "Aircraft Control and Simulation," John Wiley, 1992.

[17] H. Wang and J. Sun, "Modified model reference adaptive control with saturated inputs," In Conf. on Decision and Control, pp. 3255–3256, 1992.

[18] D. G. Ward, J. F. Monaco and M. Bodson, "Development and flight testing of a parameter identification algorithm for reconfigurable control," AIAA J. of Guidance, Control, and Dynamics, Vol. 21(6): 948–956, 1998.

Table 1: Simulation Parameters: The first row of cells defines the parameters of the model. The second and third rows of cells define controller parameters. The fourth row of cells defines the state constraints and saturation limits.

Parameter:	L_o	L_α	M_o	M_Q	M_δ
Value:	-0.1	1.0	0.1	-0.02	1.0
Parameter:	Γ_1	Γ_2	Γ_3	Γ_4	Γ_5
Value:	0.4	16.0	4.0	20.0	30.0
Parameter:	k_γ	k_α	k_Q		
Value:	1.3	3.0	30.0		
Parameter:	α_c^L	α_c^U	Q_c limits	δ_c limits	
Value:	-8.0 deg	15 deg	$\pm$ 15 $\frac{deg}{s}$	$\pm$ 45 deg	

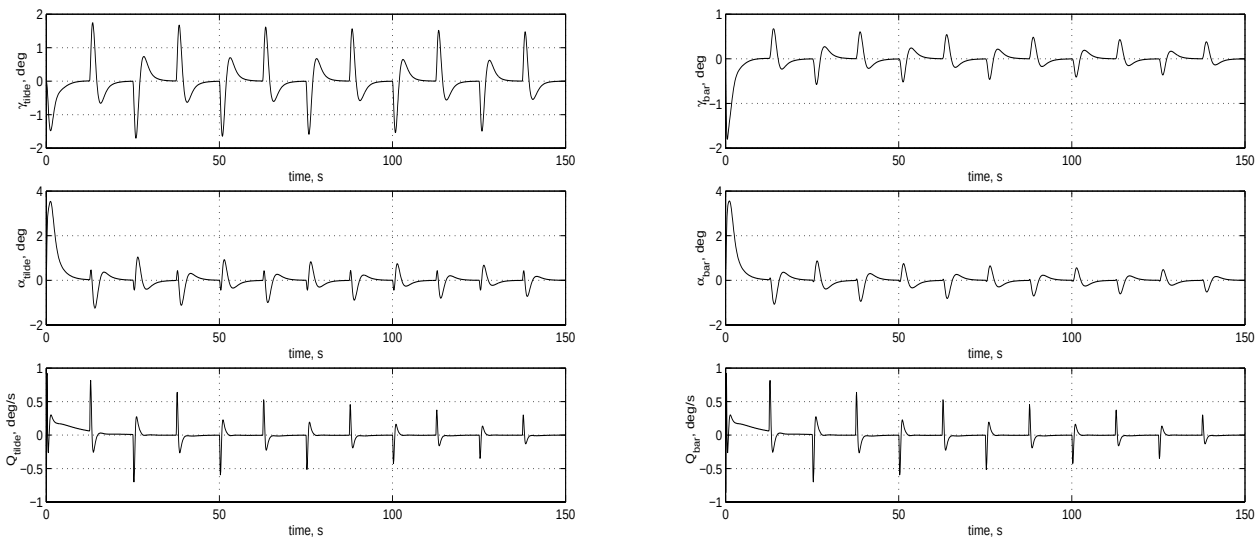

(a) Tracking errors $\tilde{x}$.

(b) Tracking errors $\bar{x}$.

Figure 2: Plots of the aircraft tracking errors for $\gamma_r \in \pm 5$ deg.

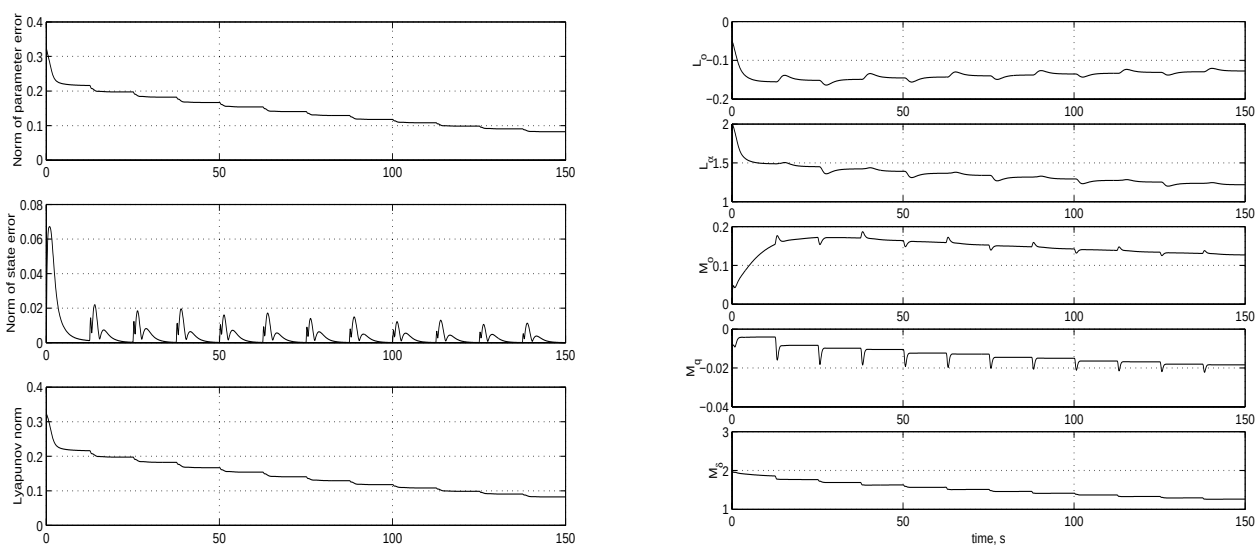

(a) Lyapunov quantities.

(b) Parameter estimates.

Figure 3: For $\gamma_r \in \pm 5$ deg: Left top - Plot of $\sqrt{\tilde{\Theta}(t)^T \Gamma^{-1} \tilde{\Theta}(t)}$ versus t. Left middle - Plot of $\|\bar{x}\|$ versus t. Left bottom - Plot of $\sqrt{\mathcal{V}(t)}$ versus t. Right - Plots of each component of $\hat{\Theta}$ versus t.

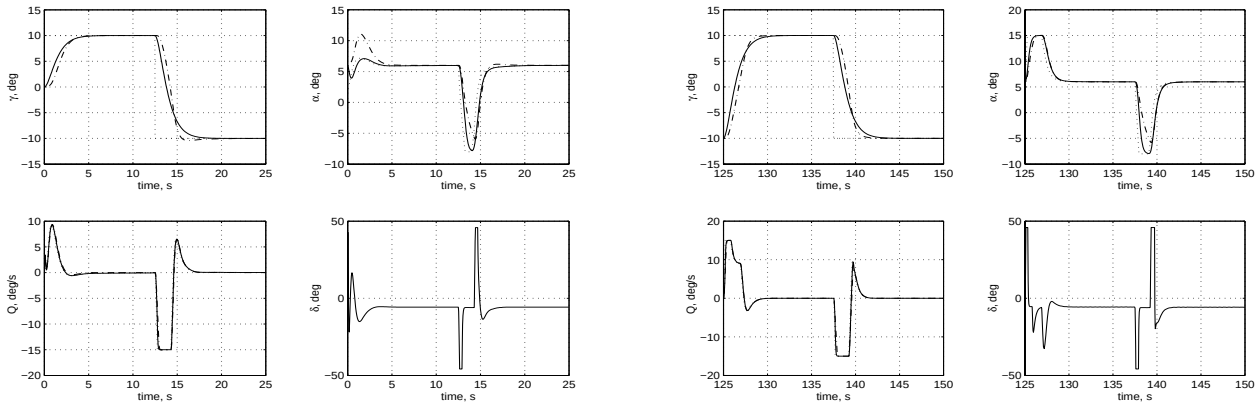

(a) Initial state and control

(b) Final state and control

Figure 4: Plots of the aircraft state and control at the beginning and end of a 150 s simulation for $\gamma_r \in \pm 10$ deg: magnitude limited command (dotted), filtered command (solid), actual (dashed)

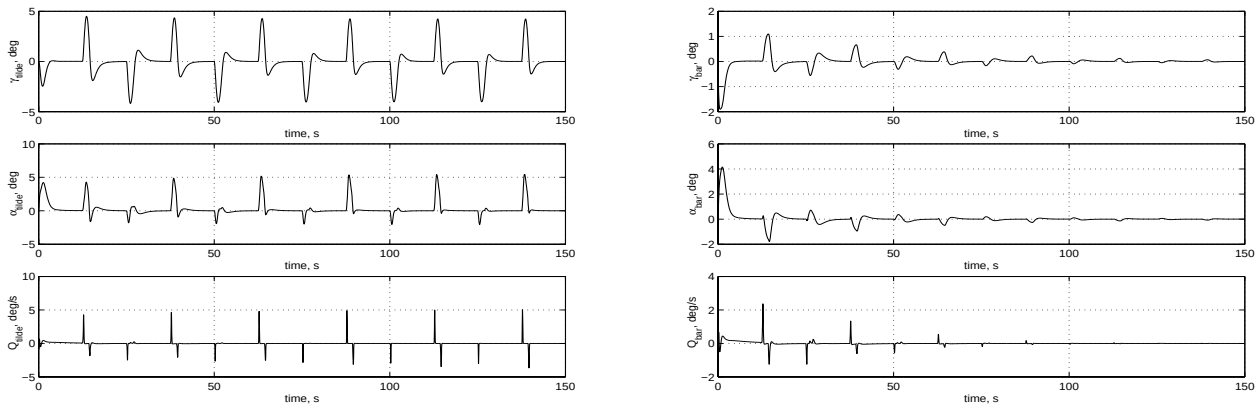

(a) Tracking errors $\tilde{x}$.

(b) Tracking errors $\bar{x}$.

Figure 5: Plots of the aircraft tracking errors for $\gamma_r \in \pm 10$ deg.

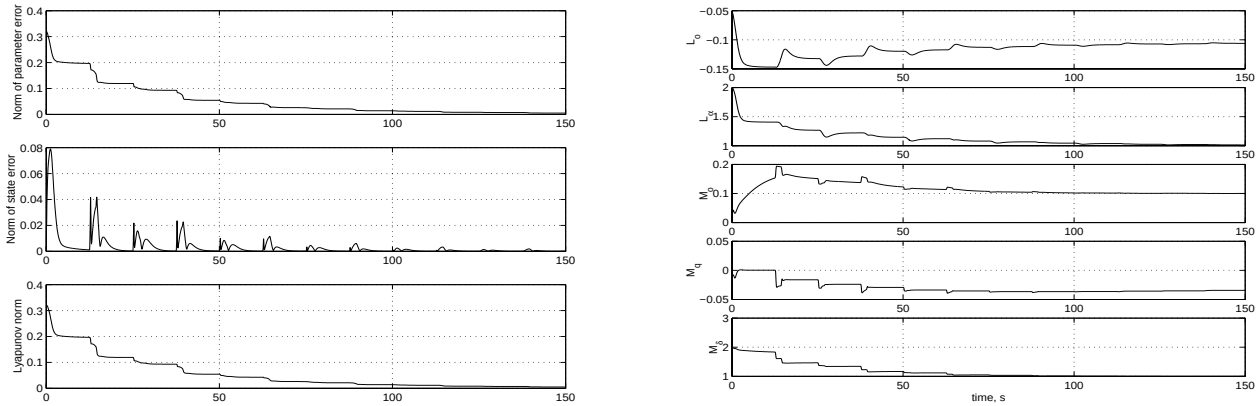

(a) Lyapunov quantities.

(b) Parameter estimates.

Figure 6: For $\gamma_r \in \pm 5$ deg: Left top - Plot of $\sqrt{\tilde{\Theta}(t)^T \Gamma^{-1} \tilde{\Theta}(t)}$ versus t. Left middle - Plot of $\|\bar{x}\|$ versus t. Left bottom - Plot of $\sqrt{\mathcal{V}(t)}$ versus t. Right - Plots of each component of $\hat{\Theta}$ versus t.